ACS OMEGA

Open Access

http://pubs.acs.org/journal/acsodf

Article

Scanning Electron Microscopy and Energy-Dispersive X-ray Spectroscopy of *Staphylococcus aureus* Biofilms

Binayak Rimal, James D. Chang, Chengyin Liu, Haley Kim, Oluwatobi Aderotoye, Bernd Zechmann, and Sung Joon Kim*

Cite This: *ACS Omega* 2024, 9, 37610−37620

Read Online

ACCESS | Metrics & More | Article Recommendations | Supporting Information

ABSTRACT: Understanding the dynamics of biofilm formation and its elemental composition is crucial for developing effective strategies against biofilm-associated infections. In this study, we employed scanning electron microscopy (SEM) and energy-dispersive X-ray spectroscopy (EDS) to investigate the morphological changes and elemental compositions of *Staphylococcus aureus* biofilms. SEM images revealed distinct stages of biofilm development, from initial aggregation to the formation of mature and aged biofilms. EDS analysis consistently showed elevated levels of sodium (Na), oxygen (O), and phosphorus (P) in the biofilm matrix, indicating its high negative charge and the presence of anionic biopolymers. The incorporation of extracellular DNA (eDNA) into the biofilm matrix, leading to significant retention of sodium ions, underscored the importance of electrostatic interactions in biofilm formation and stability. Our findings highlight the potential of EDS analysis in quantifying elemental compositions and elucidating the role of anionic biopolymers in biofilm development.

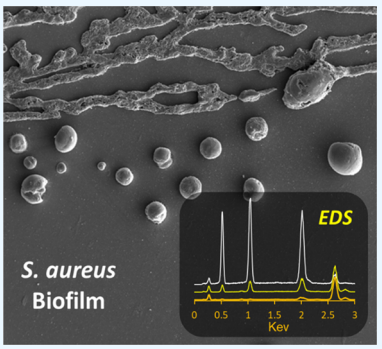

INTRODUCTION

Staphylococcus aureus is the leading Gram-positive pathogen associated with nosocomial infections related to biofilm formation.[1] Biofilm-embedded bacteria are protected from environmental threats, including antimicrobial agents, making them difficult to eradicate and serving as reservoirs for recurrent infections. For instance, *S. aureus* biofilms on an indwelling catheter can translocate to prosthetic devices, implants, cardiac valves, bones, and joint replacements.[2] These biofilm-related secondary infections are challenging to treat with conventional antimicrobial chemotherapy, as bacteria entrenched within the biofilm are intrinsically resistant to antibiotics.[3] Especially, biofilm-related infection by multi-drug-resistant *S. aureus* (MRSA) poses an extreme challenge, often requiring surgical removal of implants. Therefore, inhibiting biofilm formation and sterilizing mature biofilms are of critical clinical importance.

Biofilm formation involves multiple stages: attachment, maturation, and detachment.[1] Planktonic bacteria initiate biofilm formation by attaching to biotic or abiotic surfaces through van der Waals, electrostatic, and hydrophobic interactions.[4] In addition, bacteria can target the host matrix proteins through receptor-mediated protein interactions.[1] These surface proteins are anchored to the cell wall[5] and play significant roles in these processes. Surface proteins on the bacteria include microbial surface-recognizing adhesive matrix molecules (MSCRAMMs),[6] *S. aureus* surface protein G,[7] extracellular matrix binding protein,[8−10] protein A,[11] fibrinogen-binding proteins,[12] and biofilm-associated proteins (BAP).[13] In *S. aureus*, of the twenty-one known surface proteins containing LPXTG motif,[14] targeting signal for sortase A,[15] 11 are known to be involved in cell attachment, clumping, and biofilm formation.[16] During biofilm maturation, extensive, sortase A-mediated protein attachment occurs at the C-terminus of the cell wall's pentaglycine bride units of un-cross-linked peptidoglycan. Solid-state NMR analysis of *S. aureus* strain SA113 has shown that in planktonic bacteria, approximately 20% of pentaglycyl bridges are un-cross-linked. These are the sites for sortase A-mediated surface protein attachment. While none of the un-cross-linked bridge units in planktonic bacteria have surface proteins attached, in mature biofilms, about 25% of these sites have covalently attached surface proteins,[17] indicating substantial cell surface decoration.

In addition to proteins, biofilms are held together by extracellular polymeric substances,[18] including polysaccharides like poly-*N*-acetyl glucosamine (PNAG)[19] and wall teichoic acids (WTA) and extracellular DNA (eDNA).[20] PNAG is a positively charged polysaccharide found with approximately 20% deacetylation in *S. aureus*.[20,21] In contrast, WTA is an anionic polymer consisting of repeating polyribitol-phosphate.

Received: February 5, 2024
Revised: June 6, 2024
Accepted: July 1, 2024
Published: August 27, 2024

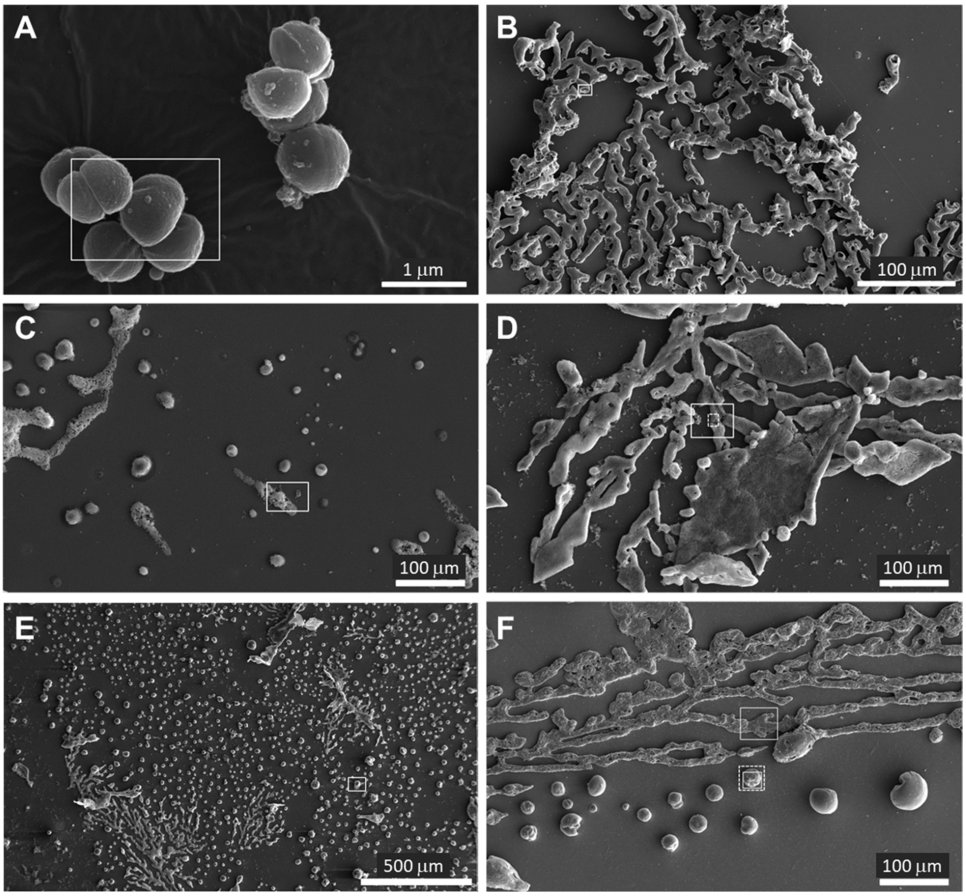

Figure 1. SEM images of *S. aureus* (SA113) grown under biofilm-inducing conditions. (A) Planktonic bacteria during the midexponential growth phase. The enlarged image corresponding to the white box is shown in Figure S1. (B) Newly formed biofilm during the midexponential growth phase. The enlarged image of the biofilm with encapsulated bacteria is shown in Figures S2−S5. (C) Biofilm at the beginning of the stationary growth phase. The empty biofilm matrix, following bacterial detachment, displays porous and wrinkled structures (Figures S6−S9). (D) Biofilm matrix after 12 h of incubation in the stationary growth phase. The mature biofilm shows detachment and dispersion of bacteria from the matrix (Figure S10−S13). (E) Mature biofilm matrix after 24 h of incubation in the stationary growth phase (Figure S14−S18). (F) Aged biofilm matrix after 48 h of incubation in the stationary growth phase (Figures S19−S22). The white boxes embedded within the figures represent magnified areas where some of the EDS analyses were performed.

WTA is covalently bonded to the C6 hydroxyl of MurNAc in the peptidoglycan of the cell wall. In *S. aureus*, WTA is abundant, constituting approximately 60% of the dry cell wall mass.[22] WTA plays an essential role in biofilm formation, as WTA-deficient *S. aureus* has a reduced ability to form biofilms.[23,24] Additionally, charge modification by the attachment of ester-linked D-Ala to the ribitol of WTA is critical for biofilm formation. The ester-linked D-Ala to ribitol neutralizes the negatively charged phosphate in WTA by introducing a positively charged amine group. A mutant impaired in ester-linked D-Ala attachment WTA fails to form biofilms and exhibits diminished virulence.[23,24,24−26] Another important anionic polymer found in *S. aureus* biofilms is extracellular DNA (eDNA).[27,28] The incorporation of eDNA into the biofilm matrix contributes to the overall structural stability of the biofilm by interacting with other polysaccharides and proteins to form a polymer network[20,29,30] resembling a grid-like structure.[31]

Characterization of biofilms has been challenging due to their complexity, heterogeneity, and size, which are often incompatible with conventional spectroscopic methods. Thus, biofilm characterization heavily relies on genetics and imaging methods.[32−35] While these approaches have provided extensive morphological insights, they lack detailed chemical and structural insights at the molecular level. Investigation using confocal laser scanning microscopy (CLSM) combined with Raman spectroscopy[30] has shown that biofilm chemical composition is dynamic. Even in static conditions where there were no detectable morphological changes in biofilms, observed by CLSM, substantial changes in the biofilm's chemical composition were detected using Raman spectroscopy. As biofilms undergo morphological changes during attachment, growth, maturation, and disassembly, understanding the chemical changes associated with these transitions is crucial.

Two spectroscopic methods that provide elemental analysis of biofilms are energy-dispersive X-ray spectroscopy (EDS) and X-ray fluorescence (XRF). Briefly, EDS analysis involves detecting X-ray emission from the atoms when a high-energy electron beam is focused on a sample. The incident high-energy electron displaces an inner-shell electron of an atom, causing a secondary outer-shell electron to fill the inner-shell vacancy, accompanied by X-ray emission. Elements are identified by measuring the ionization energy of the emitted X-rays against the known characteristic X-rays of the transitions. Quantitative analysis can be carried out by

https://doi.org/10.1021/acsomega.4c01168
ACS Omega 2024, 9, 37610−37620

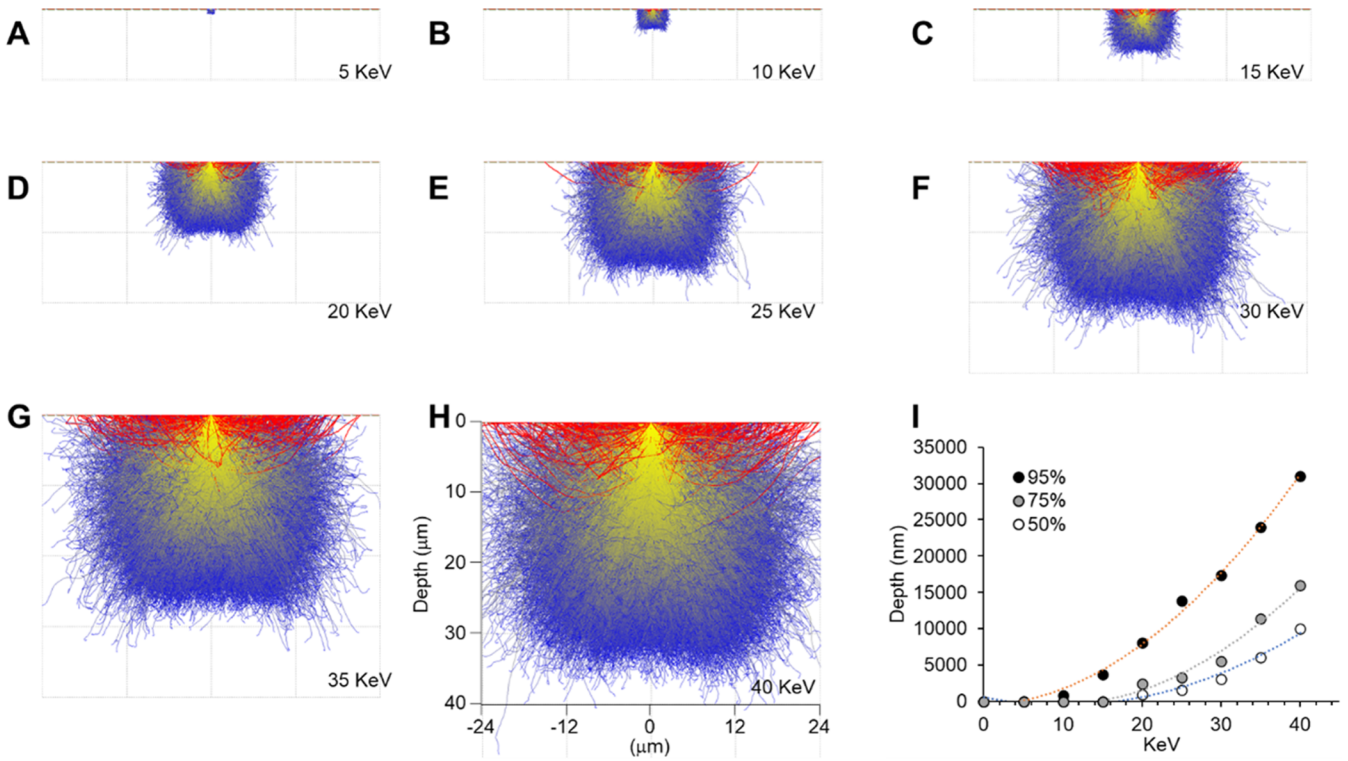

Figure 2. Monte Carlo simulations of electron trajectory analysis for a bacterial biofilm. The simulations were conducted for a bacterial biofilm with the empirical formula $C_4H_7O_2N$. A 20 nm thick Ir layer was sputtered onto the biofilm, which had a thickness of 500 μm and was placed on top of a poly(vinyl chloride) (PVC) substrate. The simulation involved 20,000 electron trajectories with an SEM beam radius of 5 nm. The electron trajectories were simulated for acceleration voltages ranging from 5 to 40 keV, as illustrated in panels (A) through (H). The red color represents the trajectories of backscattered electrons. The absorbed electron trajectories are color-coded using a gradient from yellow (high energy) to blue (low energy). The minimum electron energy for terminating the trajectory simulation was set at 0.05 keV. The corresponding heatmap depicting the depth and lateral distribution of absorbed electrons can be found in Figure S23. Panel (I) displays the maximum penetration depths plotted as a function of electron acceleration voltage for the X-ray emissions from 50% (open circles), 75% (gray circles), and 95% (closed circles) of the simulated electrons.

measuring the X-rays' ionization energies and their intensities, enabling the detection of the elemental compositions. Like EDS, XRF detects the X-ray emissions from elements for its identification, but instead of the electron beam to eject inner-shell electrons, XRF utilizes a high-energy X-ray to generate the secondary X-ray. The XRF is highly versatile and has greater sensitivity than EDS, but it has lower spatial resolution. For EDS, an electron beam can be focused to nanometer spatial resolution, whereas tens of micrometers can be focused for XRF. Another key feature of EDS is that the penetration depth of the electron beam can be adjusted to provide elemental analysis of the surface, whereas in XRF, the transmittance of X-ray provides the elemental composition of the bulk sample.

In this study, we examine the SA113 biofilm formation on poly(vinyl chloride) (PVC) substrate using scanning electron microscopy (SEM) in tandem with energy-dispersive X-ray spectroscopy (EDS). *S. aureus* readily forms a biofilm on the surface of PVC, which is commonly used in medical devices due to its flexibility, resistance to tears and scratches, ease of sterilization, and biocompatibility. PVC-based medical devices include disposable blood and biofluid-related products, such as tubing for catheters, cannulae, endotracheal, dialysis, and urethral catheters. The key advantage of combining is that SEM provides high-resolution images of surface morphology, while EDS offers elemental composition analysis at nanometer resolution of the surface. Using Monte Carlo simulations of electron trajectories in solids (CASINO),[36] we optimized the electron acceleration voltage for accurate surface analysis by limiting the focused electron beam penetration depth to a range of 0.6−1 μm. This ensured that the observed X-ray emissions are from the surfaces of bacteria and the biofilm matrix, not of the bulk sample. This combined SEM and EDS approach enables us to characterize dynamic changes in the elemental composition as *S. aureus* transitions from planktonic bacteria to mature biofilms.

RESULTS

Morphology of Biofilms. SEM images of *S. aureus* (SA113) growth under biofilm-inducing conditions reveal the dynamic development of the biofilm over time (Figure 1). During midexponential growth, a mixture of planktonic bacteria (Figures 1A and S1) and an early biofilm (Figures 1B and S2) is observed. Enlarged views of the newly formed biofilm (Figures S3−S6) show a dense, smooth matrix encapsulating the bacteria. As the growth progresses into the stationary phase, the biofilm surface becomes rough and exhibits wrinkle-like appearances with visible holes (Figures 1C and S6−S9). The biofilm appears partially digested, with some bacteria detaching from the bottom (Figures S8 and S9), indicating biofilm detachment. Some detached bacteria aggregate to form clusters on the surface (Figure S9).

A mature biofilm, after 12 h poststationary growth phase, shows a mix of empty matrix, detached bacteria, and newly

https://doi.org/10.1021/acsomega.4c01168
ACS Omega 2024, 9, 37610−37620

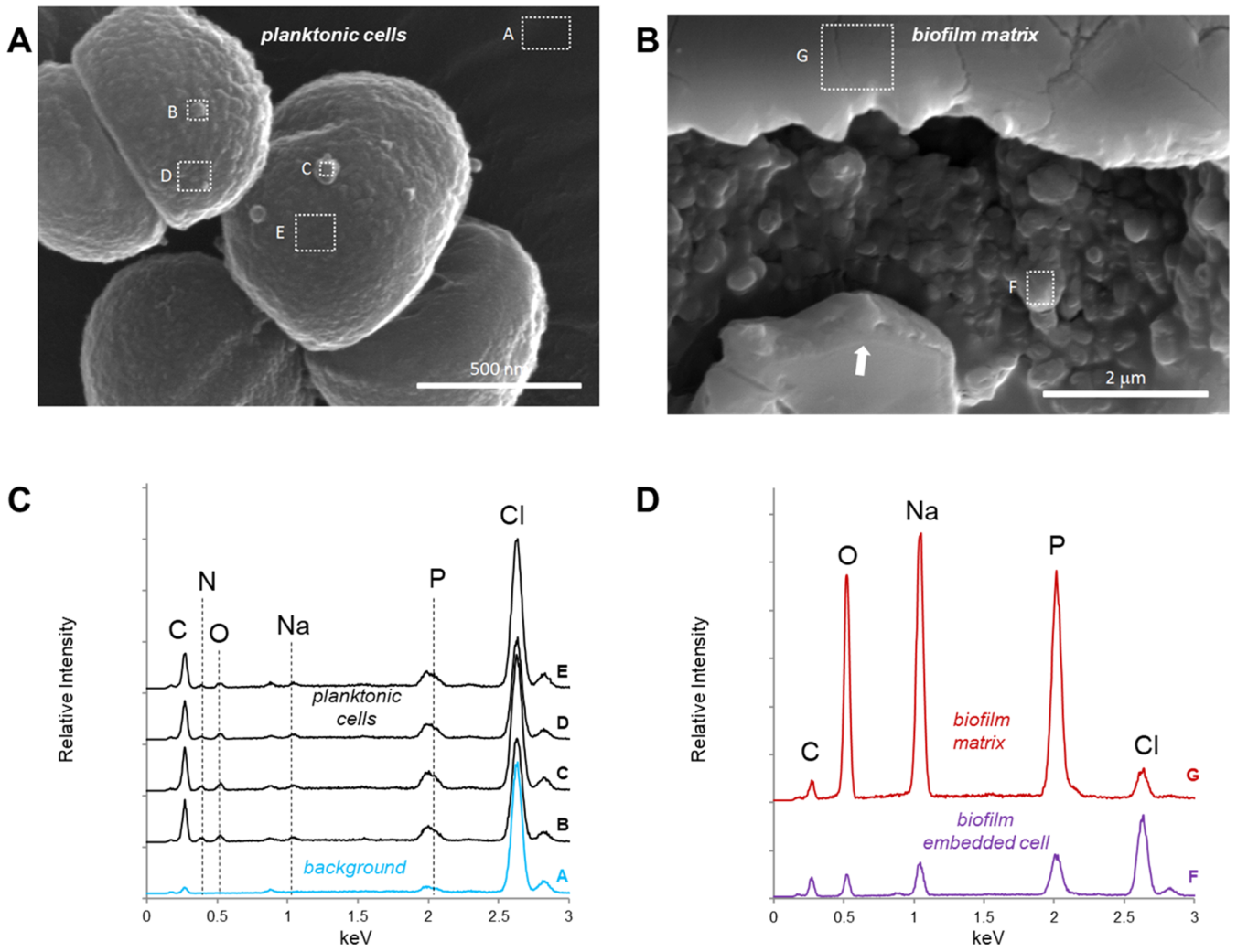

Figure 3. SEM images of planktonic *S. aureus* (A) and the biofilm (B) grown on a PVC slide during the midexponential growth phase. A white arrow in panel B shows a smooth biofilm matrix that encapsulates the bacteria within the biofilm. EDS spectra were acquired from specific spots marked by dotted squares with letter designations. Panel (C) presents the EDS spectra of the PVC slide (blue spectrum), and planktonic bacteria (labeled B−E) are shown in panel (C). In panel (D), the EDS spectra of bacteria embedded within the biofilm matrix (purple spectrum) and the biofilm matrix itself (red spectrum) are displayed.

formed bacterial clusters (Figure 1D). Magnified images (Figures S10−S13) reveal dispersed bacteria due to partial biofilm degradation, with prominent wrinkled features on the surface. SEM images after 24 h show various stages of biofilm formation (Figure 1E and Figures S14−S18). The detachment process results in a rough and porous appearance, primarily composed of the matrix (Figure S15), while some planktonic bacteria initiate reattachment and continue to grow (Figures S16−S18).

An aged biofilm, 48 h after stationary growth phase, shows a near absence of planktonic bacteria (Figure 1F). Instead, visibly thick layers of branched biofilm layers are observed on the PVC surface (Figures S19−S22). Additionally, large spherical clusters of biofilms are found on the surface. We speculate that shaking the culture at 60 rpm during incubation caused bacterial aggregates to form spherical clusters without surface attachment, whereas the branched biofilm likely resulted from bacteria growing on the PVC surface. These observations illustrate the complex and dynamic nature of biofilm development in *S. aureus* over time, highlighting the transition from planktonic bacteria to mature, structured biofilms.

Monte Carlo Simulation of Electron Trajectory in Solids (CASINO). CASINO[36] was used to calculate multiple electron trajectories for EDS under various biofilm configurations and electron beam energies. To represent iridium (Ir) sputter-coated biofilm grown on a surface of PVC, three sample layers were simulated: (i) a 20 nm Ir layer, (ii) a 500 μm layer of general microbial cells and biofilm represented by an empirical formula $C_4H_7O_2N$ or $C_4H_7O_2NP$, and (iii) PVC substrate. Simulations were conducted for 20,000 electron trajectories, using a focused electron beam radius set at 5 nm, with an acceleration voltage varying from 5 to 40 keV for every 5 keV interval. The simulated electron trajectories for the biofilm represented by the empirical formula $C_4H_7O_2N$ are shown in Figure 2.

Heatmaps illustrating the depth and lateral distribution of absorbed electrons are presented in Figure S23. The maximum sample depth penetrations with 50, 75, and 95% of all electrons are plotted against the acceleration voltage (Figure 2I). For beam energies of 5 and 10 keV, nearly all electron energy losses

https://doi.org/10.1021/acsomega.4c01168
ACS Omega 2024, 9, 37610−37620

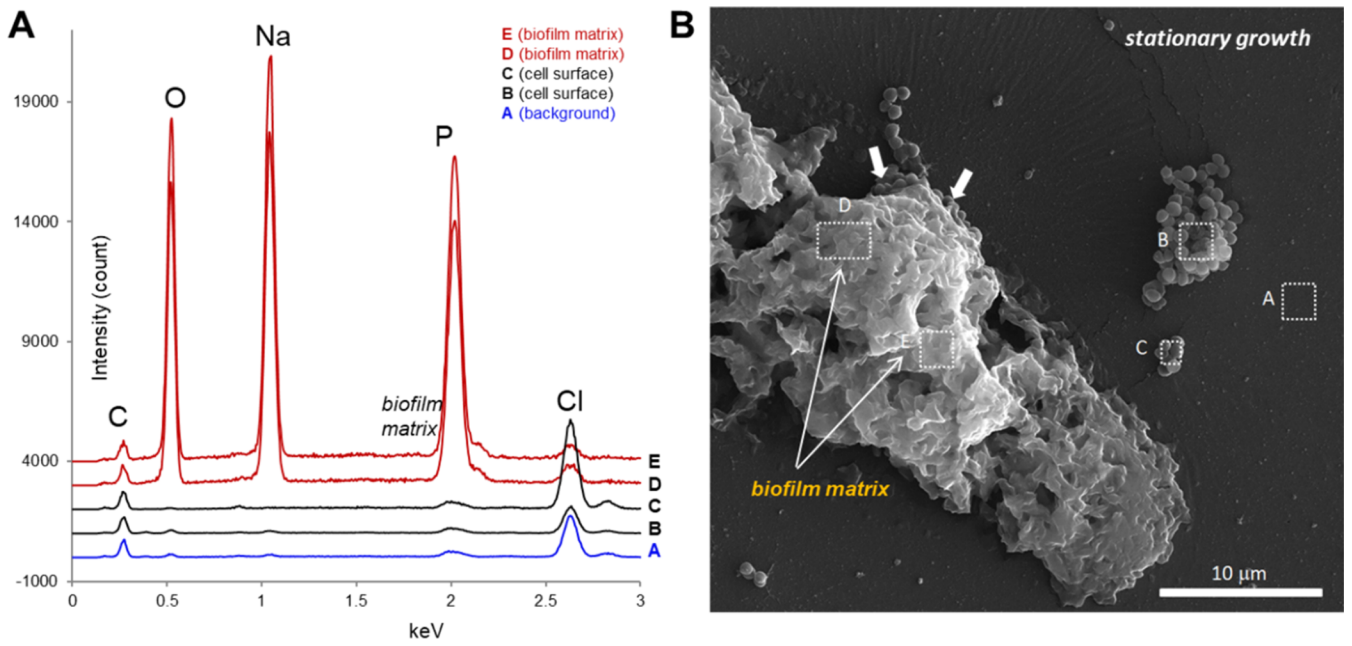

Figure 4. SA113 biofilm at the onset of the stationary growth phase. During the early stages of the stationary growth phase, EDS spectra (A) were collected from specific spots indicated by dotted squares with letter designations shown in the SEM image of the SA113 biofilm (B). The white arrows indicate the bacteria emerging from the mature biofilm. The EDS spectrum of the bare PVC substrate is labeled as A (blue spectrum); the spectra of planktonic bacteria are denoted as B and C (black spectra); and the EDS spectra of the biofilm matrix are identified as D and E (red spectra).

occurred within the sputtered Ir layer above the biofilm. Increasing the energy to 15 keV did not substantially enhance electron penetration into the biofilm, with approximately 75% of the total energy losses occurring within the Ir layer. For 30 keV electron beams, 75 and 50% of energy losses occurred within depths of 6 and 3 μm, respectively. With a 40 keV electron beam, 75 and 50% of energy losses were within depths of 16 and 10 μm, respectively. For electron beams with energies of 20 keV, optimal electron penetrations with approximately 75 and 50% of energy losses occurring within depths of 2 and 0.9 μm were observed.

Additional CASINO simulations were performed for samples containing elemental phosphorus, characterized by the empirical formula $C_4H_7O_2NP$ of 500 μm in thickness. The electron trajectories and corresponding heatmaps are illustrated in Figures S24 and S25, respectively. These simulations revealed that the K-shell transitions of phosphorus dominate the X-ray emissions, resulting in reductions in relative X-ray emissions from carbons, oxygens, and nitrogens. The simulated intensities of electron absorption as a function of depth penetration for samples with empirical formulas $C_4H_7O_2N$ and $C_4H_7O_2NP$ at an electron acceleration voltage of 20 keV are shown in Figure S26. CASINO simulations showed that the penetration depth of the focused electron beam was not affected by the presence of phosphorus in the biofilm.

EDS Analysis of the Newly Formed *S. aureus* Biofilm. SEM images of *S. aureus* harvested during the midexponential growth phase display the presence of both planktonic bacteria (Figure 3A) and the newly formed biofilm (Figure 3B). These images are enlarged views of white boxes shown in Figure 1A,1B. Planktonic bacteria undergoing cell division show rough cell surfaces with distinct features. In contrast, the biofilm-embedded bacteria, visible only through occasional openings in the biofilm (Figures S4 and S5), exhibit a smooth surface and have sizes significantly less than 500 nm in diameter. The surface of the newly formed biofilm is smooth and featureless, contrasting the rough surfaces found in the mature and aged biofilms.

The locations of the focused electron beam from which the EDS spectrum was collected are each marked in the figure using a dotted square with letter designations (Figure 3A through D). Spot A focuses the beam on the PVC substrate; spots B−E focus on various cell surface features of the planktonic bacteria; spot F focuses on bacteria encased within the biofilm matrix; and spot G focuses on the outer smooth surface of the biofilm matrix. The corresponding EDS spectra for each spot are presented in Figure 3C,D. As the bacteria were cultured on the top of poly(vinyl chloride) (PVC), the EDS spectrum of the substrate surface without *S. aureus* cells is dominated by the chlorine X-ray emission observed at 2622 eV (Figure 3C, spectrum A). A thin organic layer deposited on top of the substrate also gives rise to low-intensity $K_{\alpha 1}$ X-ray emissions from carbon (277 eV), nitrogen (392 eV), and oxygen (525 eV). All EDS spectra of planktonic *S. aureus* on the surface of PVC were normalized to the chlorine X-ray emission intensity at 2622 eV (Figure 3C). For the EDS spectra of the thick layered biofilm, spectra were normalized to the carbon $K_{\alpha 1}$ X-ray emission intensity at 277 eV (Figure 3D). Identification of the elements and their corresponding X-ray emission assignments for spots E, F, and G are found in Figure S27. Figure S28 shows a detailed inspection of the Ir X-ray emissions at 1979.9 and 9175 eV, corresponding to the $M_{\alpha 1}$ and $L_{\alpha 1}$ transitions. The intensity of the Ir $L_{\alpha 1}$ transition is weak and resolved from high intensities of phosphorus $K_{\alpha 1}$ and $K_{\alpha 2}$ emissions at 2012.7 and 2013.7 eV. Therefore, the use of Ir for sputter coating of biofilm does not interfere with the X-ray emission assignment of phosphorus and other common elements found in biological systems. Moreover, the Ir coating provides an added advantage over the carbon-sputtered biofilm for EDS analysis as the intensity of carbon X-ray emission can

https://doi.org/10.1021/acsomega.4c01168
ACS Omega 2024, 9, 37610−37620

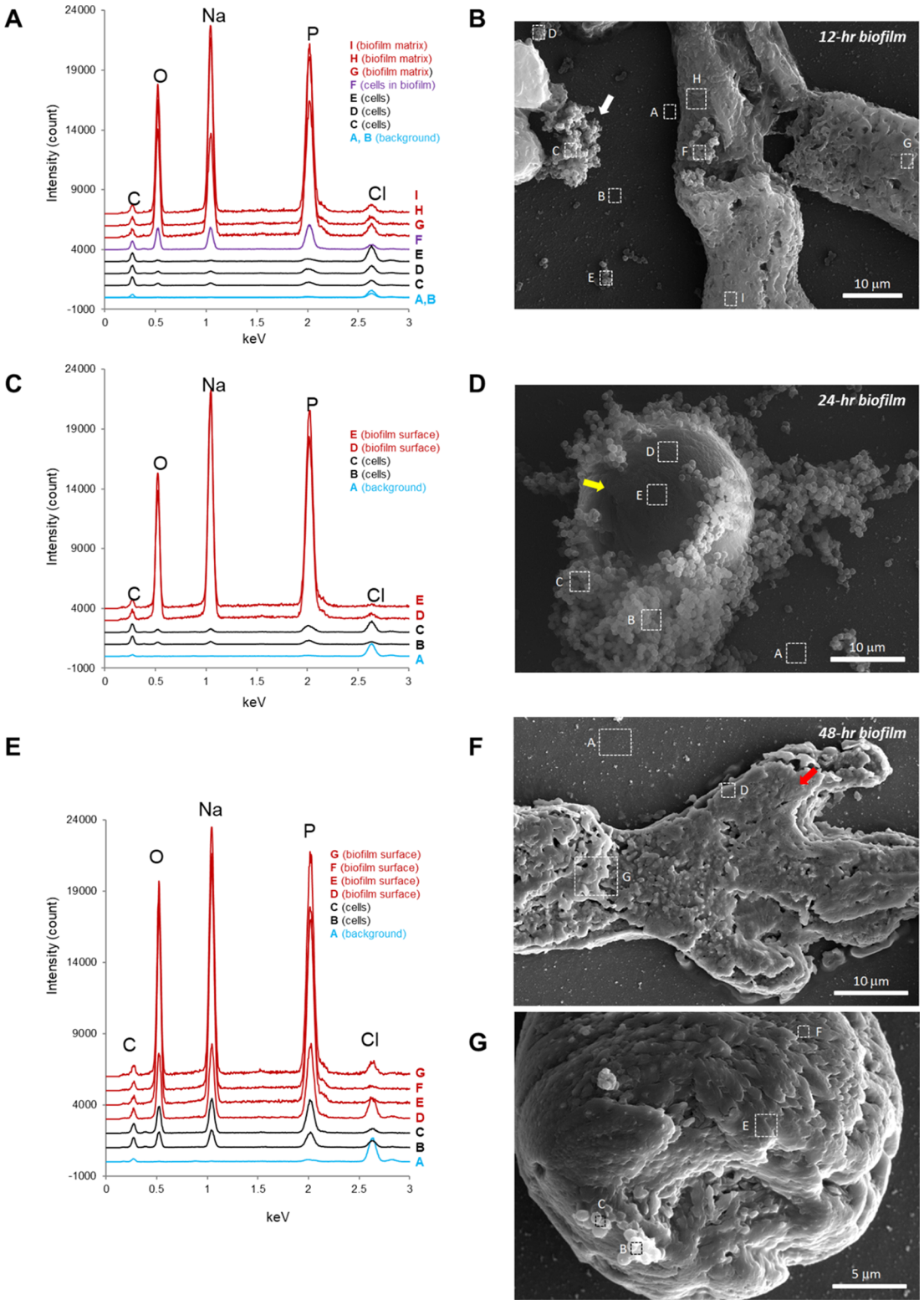

Figure 5. SA113 biofilm after 12, 24, and 48 h poststationary growth phase. In the SEM image (B) at 12 h poststationary growth phase, EDS spectra (A–I) are collected from designated spots indicated by dotted squares and letters. The spectra include the bare PVC substrate (A and B, blue spectra), planktonic bacteria (C, D, and E, black spectra), bacteria on the biofilm matrix surface (F), and the biofilm matrix (G, H, and I, red spectra). In the SEM image (B) at 24 h poststationary growth phase, EDS spectra (A–E) are collected from spots marked by dotted squares and letters. This newly formed biofilm exhibits a smooth surface with attached cell clusters. In the SEM image (F and G) at 48 h poststationary growth phase, EDS spectra (A–G) are collected from designated spots indicated by dotted squares and letters. The white arrow in panel B marks a cluster of planktonic bacteria that are beginning to form the biofilm as they are covered with an extracellular matrix. The yellow arrow in panel (D) marks a smooth surface of the newly formed biofilm. The red arrow in panel F marks the aged biofilm.

https://doi.org/10.1021/acsomega.4c01168
ACS Omega 2024, 9, 37610–37620

be utilized for normalization, whereas for carbon-sputtered samples, similar normalization would not be feasible.

The EDS spectra of planktonic bacterial cell surfaces (spots B−E) show emission lines from C, N, O, Na, P, and Cl (Figure 3C). A significant Cl emission originating from the PVC is also visible, as the electron beam with an acceleration voltage of 20 keV can penetrate through a single layer of planktonic layers and into the PVC layer (Figure 2I). The intensity of the phosphorus X-ray emission, centered at 2013.7 eV, is significantly less than that of C emission and overlaps with the Ir emission at 1979.9 eV (Figure S28). The EDS spectrum of the bacterium embedded within the biofilm (Figure 3D, purple spectrum) shows an increase in the X-ray emissions from O, Na, and P. In comparison, the EDS of the biofilm matrix (Figure 3D, red spectrum) shows dramatic increases of the emission of O at 525 eV, Na emissions ($K_{\alpha 1}$ and $K_{\alpha 2}$) at 1041 eV, and P emissions at 2014, 1013, and 2139 eV. Emissions from Na and P have broader peaks due to multiple transitions ($K_{\alpha 1}$, $K_{\alpha 2}$, and K_{b1}) with similar energies. Notably, the relative emission intensity ratio of Cl to C is lower compared to the planktonic and biofilm-encapsulated bacteria, attributed to the increased depth of the biofilm elevated away from the PVC substrate.

The X-ray emission ratios of C to O, C to Na, and C to P increase from planktonic bacteria to bacteria encapsulated in biofilms and to biofilm matrix. The phosphorus content of the biofilm matrix is approximately 40 times greater than that of planktonic bacteria, while bacteria embedded within the biofilm matrix show phosphorus 6 times greater than that of planktonic bacteria. Similarly, the oxygen content of the biofilm matrix is approximately 77-fold greater and 8-fold greater for bacteria embedded within the biofilm matrix, compared to planktonic bacteria. Finally, sodium showed the largest increase, being 180-fold greater in the biofilm matrix and 16-fold greater in embedded bacteria relative to sodium found in planktonic bacteria.

EDS Analysis of the Mature *S. aureus* Biofilm. *S. aureus* harvested at the stationary growth phase shows a mature biofilm with planktonic bacteria that are liberated from the biofilm (Figure 4). SEM images of biofilm matrix surfaces, unlike those in the midexponential phase, are rough and filled with holes (Figures S6 and S7). Although the biofilm appears empty, some encapsulated bacteria are visible near the surface interface between the PVC and the biofilm matrix. Some of the escaped planktonic bacteria form small clusters of aggregates on the surface of the PVC substrate (Figures 4B and S8−S9).

EDS spectra were collected by directing the electron beam to various regions of the mature biofilm matrix. Spot A is the PVC substrate (background), spots B and C correspond to planktonic bacteria clusters, and spots D and E correspond to the biofilm matrix (Figure 4B). The EDS spectra of the mature biofilm (Figure 4A, redline) for spots D and E show an increase in X-ray emissions from O, Na, and P compared to planktonic bacteria (Figure 4A, black lines).

EDS Analysis of the Aged *S. aureus* Biofilm. SEM images and EDS spectra of *S. aureus* biofilms at 12, 24, and 48 h poststationary growth are shown in Figure 5. As the *S. aureus* culture progressed beyond the stationary growth phase, it exhibited a mix of aged biofilms with wrinkled and puckered surfaces (Figures S14, S15, and S18), planktonic bacteria (Figure S17), and the newly formed biofilm (Figure 5D). The selected regions for EDS spectra were acquired and marked with dotted boxes (Figure 5B,C).

Regardless of the biofilm's age, the EDS spectra of all planktonic cells, whether directly above the PVC substrate or on top of the aged biofilm, closely resembled the EDS spectrum of planktonic cells harvested during the midexponential growth phase (Figure 3C). Conversely, the EDS spectra of the biofilm matrix, whether newly formed (Figure 2), matured (Figure 4), or aged (Figure 5), all exhibited distinct increases in the elemental compositions of O, Na, and P.

DISCUSSION

Biofilm Morphology. The *S. aureus* strain SA113 is known for its robust biofilm-forming capabilities, especially in the presence of excess glucose.[37,38] To cultivate SA113 biofilm, we placed a PVC microscope coverslip into a 50 mL conical polypropylene centrifuge tube containing 10 mL of trypticase soy broth (TSB) supplemented with 1% glucose. The culture was incubated at 37 °C with a continuous slow circular motion at 60 rpm. During the exponential growth phase (3 to 4 h of growth), SA113 formed visible aggregates, resulting in large particulate suspensions. Biofilms grown on the surface of the PVC coverslip showed the attachments of both planktonic bacteria and the newly formed biofilms. The newly formed biofilm displayed a branching pattern (Figure 1B), likely due to the sheer force from the shaking motions. A close examination showed a smooth surface with occasional openings exposing encapsulated bacteria deep within the biofilm (Figure 3B). This smooth biofilm matrix, approximately 1 μm in thickness (Figure 3B, white arrow), appeared to be devoid of bacterial cells.

As growth progresses into the stationary growth phase (Figure 4), the biofilm morphology evolved, losing its smooth appearance and becoming uneven, rough, and wrinkled. Visible holes in the matrix indicated biofilm degradation as bacteria emerge from within. Some partially encapsulated bacteria regained their normal size and shape as they emerged from the biofilm (Figure 4b, white arrows). Escaped planktonic bacteria clustered and attached to the substrate, initiating new biofilm formation. Aged biofilms collected at 12, 24, and 36 h of poststationary phase exhibited a mixed presence of clustered planktonic bacteria, newly formed immature biofilm with partial matrix formation (Figure 5B, white arrow), and aged biofilm (Figure 5F, red arrow). Additionally, two distinct shapes of biofilms were visible in mature and aged biofilms: branching-patterned and spherical-shaped biofilms. The branching-patterned biofilm shows extensive surface attachment to the substrate, suggesting that this pattern results from the continual growth of surface-attached bacteria. In contrast, the spherical-shaped biofilm resulted from bacterial aggregation formed in suspension, without surface attachment, shaped by the sheer force exerted by continual circular motion during the growth.

CASINO Simulation to Optimize the Electron Beam Penetration Depth. EDS analysis provides high spatial resolution due to the electron beam's ability to focus to a 5 nm radius. However, a critical challenge in EDS analysis of biofilms is ensuring that the electron beam does not penetrate too deeply, which would result in a bulk composition that combines the elemental compositions of both the biofilm matrix and the bacteria. Our goal was to optimize the electron acceleration voltage to limit the depth of electron beam penetration to approximately 1 μm, the observed thickness of the newly formed biofilm matrix shown in the SEM image of Figure 3B (white arrow). To achieve this, we used CAINO

https://doi.org/10.1021/acsomega.4c01168
ACS Omega 2024, 9, 37610−37620

simulations to model electron trajectories incident on the biofilm sample. The simulated biofilm sample consisted of three layers of different materials. The first layer was 20 nm of iridium, corresponding to Ir sputtered on biofilm samples for SEM imaging. The second layer, 500 μm thick, represented microbial cells using an empirical formula $C_4H_7O_2N$ or $C_4H_7O_2NP$. The third layer was a PVC substrate with an empirical formula C_2H_3Cl.

The optimal electron beam penetration depth was determined for an electron acceleration voltage at 20 keV. Under this condition, CASINO simulation showed that approximately 50% of the electron absorption occurred within 0.9 μm of the surface. This was subsequently confirmed as EDS spectra of a single planktonic bacterium placed directly on top of the biofilm matrix (Figure 5G, spots C and B; Figure 5B, spot F) at 20 keV showed an elemental composition consistent with planktonic bacteria on PVC, with a minor contribution from the biofilm matrix. Additionally, EDS spectra with the electron beam focused on a cluster of bacteria, consisting of only a few layers on the top of the biofilm matrix (Figure 5D, spots C and B), were identical to those of planktonic bacteria found on PVC. Therefore, at an electron acceleration voltage at 20 keV, the electron beam did not penetrate significantly beyond the depth of a single layer of bacteria. This optimization ensures the accuracy of EDS analysis in distinguishing between biofilm matrix and bacterial components, providing valuable insights into biofilm composition and structure.

EDS Analysis of Biofilms. Elemental analysis of the biofilm surface was performed by using EDS with the electron beam focused at 20 keV on various surfaces. These surfaces included individual planktonic bacteria, aggregated bacteria initiating biofilm formation without a visible biofilm matrix, bacteria encapsulated within the biofilm matrix, newly formed biofilm matrix with a smooth surface, and aged, puckered, uneven, and empty biofilm matrix.

The EDS spectra of individual planktonic bacteria and aggregated bacteria without a visible biofilm matrix revealed X-ray emissions dominated by C and P, with minor emissions of N, O, and Na. However, the appearance of the biofilm matrix covering the bacteria increased the intensities of O, Na, and P emissions more than eight, twenty-one, and 6-fold, respectively. For biofilms, regardless of their age (new, mature, and old), all exhibited dramatic increases in the intensities of X-ray emissions from O, Na, and P by as much as 77-, 180-, and 40-fold, respectively. These increases were consistently observed across all biofilm matrices, independent of their morphology.

***S. aureus* Biofilm Contains a High Concentration of Sodium Ions.** The presence of sodium ions was detected by monitoring the intensities of its emission lines ($K_{\alpha1}$, $K_{\alpha2}$, and K_{b1}) at 1041 and 1071 eV. In planktonic bacteria, the intensity of Na emission is low compared to carbon $K_{\alpha1}$ X-ray emission at 277 eV. This is a common observation in single-cell bacteria,[39] as the relative amount of Na in a bacterium is significantly lower than the more abundant elements like carbon. Additionally, the intensity of X-ray emission for each element is highly dependent on the electron acceleration voltage,[39] indicating that the weak intensities of Na X-ray emission do not necessarily imply the absence of Na ions in the sample. Similarly, the intensities of X-ray emission from C and N in an EDS spectrum do not directly correlate with their relative abundances. For instance, while the empirical chemical formula for general microbial cells represented as $C_4H_7O_2N$ indicates a C to N ratio of 4:1, the observed X-ray emission intensity for N is far smaller than a quarter of the carbon intensity. To accurately measure relative changes in Na ion content between samples, we kept the electron acceleration voltage constant and normalized the spectra to the X-ray intensity of the carbon.

Sodium ions were introduced during growth, as they were present in the TSB at a concentration of 5 g/L and were further introduced during the SEM sample preparation process. In this process, samples were fixed in a 0.06 M phosphate buffer for 90 min, followed by a phosphate-buffered saline wash. Despite both planktonic cells and biofilms being exposed to excess sodium ions, only the biofilm, regardless of its age and morphology, showed significant retention of sodium ions. The amount of Na bound to the biofilm was approximately 180-fold greater compared to the Na bound in planktonic cells. This significant retention of Na ions in the biofilm matrix strongly indicates that the matrix is highly negatively charged, whereas the planktonic cell surface remains relatively neutral. The increase in salt concentration, including sodium ions, has been shown to enhance *S. aureus* biofilm formation[40−42] and influence the mechanical properties of the biofilm.[20,43] The retention of sodium ions suggests that these ions play an important role in biofilm formation and stability by binding to the negatively charged biofilm matrix.

Increased Levels of Na, O, and P in *S. aureus* Biofilms Are Indicative of the Presence of Anionic Polymers. The EDS spectra of the SA113 biofilm revealed that the elevation in sodium emission intensity was accompanied by prominent phosphorus and oxygen X-emission lines, suggesting a significant presence of phosphate group within the biofilm matrix. Phosphate groups are key constituents of many biopolymers, including WTA and DNA, both of which are involved in biofilm formation. In *S. aureus*, WTA constitutes a major component of the cell wall, accounting for as much as 60% of its dry mass.[22] The highly negatively charged ribitol phosphates in WTA bind to various cations and contribute to cation homeostasis.[44] Moreover, WTA is essential for the attachment to abiotic surfaces[24] and the host's cells.[45] Mutant *S. aureus* lacking WTA not only exhibits reduced biofilm formation[23,24] but also shows an inability to colonize the host[45] with attenuated virulence.[46]

However, the observed increase in the elemental composition of Na, O, and P in the biofilm is not due to enhanced WTA production. Since WTA is covalently attached to the C6 hydroxyl of MurNAc in the peptidoglycan of cell walls, an increase in WTA production should correspond to an increase in Na, O, and P compositions in the EDS spectra of *S. aureus*, which was not observed. Instead, the observed increases were confined to the biofilm matrix. CASINO simulation assured that EDS spectra of biofilm acquired using an electron acceleration voltage of 20 keV prevented the contributions from the bacteria that are buried deeply within the matrix. Therefore, it is unlikely that the observed increases in Na, O, and P in the biofilm matrix are solely due to WTA.

The most probable anionic biopolymer responsible for the elevated levels of Na, O, and P in the biofilm matrix is DNA. DNA is rich in phosphate, highly negatively charged, and readily binds to sodium ions. Extracellular DNA (eDNA) is a major component of the extracellular polymeric substance found in the biofilm matrices of various bacterial species,[31,47,48] including *S. aureus*.[28,49,50] In biofilms, eDNA plays a crucial structural role, forming an electrostatic network with positively

https://doi.org/10.1021/acsomega.4c01168
ACS Omega 2024, 9, 37610−37620

charged proteins and other biofilm components.[51] This network creates a scaffold that provides mechanical stability for the biofilm structure. Disrupting this charge network by targeting eDNA or proteins can weaken the biofilm structural, as SA113 biofilm has been shown to be highly susceptible to DNase I[20] and proteinase K[37] degradation. Additionally, endolysin (phage lytic proteins that target peptidoglycan in cell walls)[52] and sodium metaperiodate,[37] which can oxidize glycans, have been shown to disrupt extracellular polysaccharides, leading to biofilm removal. Thus, the presence of Na, O, and P in the biofilm matrix suggests the involvement of anionic polymers, particularly eDNA, in *S. aureus* biofilm formation and stability.

CONCLUSIONS

In conclusion, the study utilized a combination of SEM and EDS to investigate the dynamic changes in the morphology and elemental compositions of *S. aureus* biofilms. SEM images revealed distinct morphological transitions during biofilm development, from smooth-surfaced early biofilms to uneven and puckered mature biofilms, and finally to aged biofilms with only the matrix remaining. EDS analysis in biological systems is difficult due to the similar elemental compositions of biological samples, which primarily consist of low atomic number elements such as C, N, and O. Despite this challenge, by limiting electron beam penetration to within 0.6 to 1 μm, the analysis ensured accurate representation of the elemental composition of biofilm matrix without contributions from embedded bacteria. EDS analysis consistently showed elevated levels of sodium (Na), oxygen (O), and phosphorus (P) in the biofilm matrix, indicating its high negative charge and the presence of phosphate-containing anionic biopolymers.

The increased presence of Na, O, and P was observed only for the biofilm matrix but absent from all EDS spectra of planktonic cells. Since WTA is covalently bound to the peptidoglycan in the cell walls, this ruled out the possibility of WTA being responsible for the observed changes, indicating the role of eDNA in the biofilm matrix. The incorporation of eDNA into biofilms led to the significant retention of sodium ions, as much as a 180-fold increase. As an increase in salt concentration has been shown to enhance *S. aureus* biofilm formation[40−42] and influence the mechanical properties of the biofilm,[20,43] eDNA interaction with Na ions underscores the importance of electrostatic interactions in contributing to the biofilm formation and maintaining its stability. Understanding these mechanisms provides valuable insights into potential strategies for disrupting biofilm formation and improving treatment efficacy against biofilm-associated infections.

MATERIALS AND METHODS

Scanning Electron Microscopy of Biofilms. Starter cultures of the strain SA113 were initiated by inoculating 5 mL of trypticase soy broth (TSB) in a test tube with a single colony obtained from a nutrient agar plate. These starter cultures were incubated overnight at 37 °C with continuous shaking at 200 rpm without aeration. Biofilm samples were prepared by inoculating 10 mL of TSB enriched with 1% glucose in a 50 mL conical polypropylene centrifuge tube containing a disposable PVC microscope coverslip. The culture was incubated at 37 °C with continuous slow circular motion at 60 rpm. Biofilm formed on the microscope coverslip at the midexponential growth phase was collected after 3.5 h of incubation and stationary growth sample at 8 h of incubation. Subsequent mature biofilm samples were collected after an additional 12, 24, and 48 h poststationary growth.

To fix the biofilm attached to the disposable plastic microscope coverslips (dimensions of 22 × 22 mm with 0.17 to 0.25 mm thickness), 2.5% glutardialdehyde in 0.06 M phosphate buffer (pH 7.2) was used. This buffer was prepared from sodium phosphate dibasic heptahydrate and sodium phosphate monobasic monohydrate. The samples were fixed for 90 min at room temperature, followed by four 10 min washes in the buffer.

Samples were dehydrated through a graded series of acetone, with two 10 min steps at each concentration (50, 70, 90, and 100%). After critical point drying using an EM CPD300 (Leica Microsystems, Wetzlar, Germany), the specimens were mounted on stubs and sputter-coated (EM ACE 600, Leica Microsystems) with 20 nm of iridium. Observations were made using a Versa 3D scanning electron microscope (FEI, Hillsboro, OR).

Energy-Dispersive X-ray Spectroscopy of Biofilms. Energy-dispersive X-ray spectroscopy (EDS) was conducted using an Octane Pro silicon drift detector (EDAX, Mahawah, NJ) at 20KV, with a spot size 7, and at a working distance of 10 mm. The energy of the emitted X-ray was measured by a silicon drift detector (EDAX, Mahawah, NJ), which, by measuring ionization energy, identifies the elements through known characteristic X-rays.

CASINO. Monte Carlo simulations of electron trajectory in solid were conducted using CASINO[53] (v. 2.51). The simulated sample consisted of a multilayered structure with 20 nm of iridium (Ir) sputtered onto a bacterial biofilm grown on a PVC substrate. The chemical composition of bacteria was empirically represented by $C_4H_7O_2N$ or $C_4H_7O_2NP$, with a thickness of 500 μm, while PVC was represented by C_2H_3Cl as the substrate. The beam radius was fixed at 5 nm, and 20,000 electron trajectories were calculated for each acceleration voltage, ranging from 5 to 40 keV. The minimum electron energy for terminating the trajectory simulation was set at 0.05 keV.

ASSOCIATED CONTENT

Supporting Information

The Supporting Information is available free of charge at https://pubs.acs.org/doi/10.1021/acsomega.4c01168.

SEM images of planktonic *S. aureus* and newly formed biofilm during the midexponential growth phase; SEM images of mature biofilms; SEM images of aged biofilms; CASINO simulations of electron trajectories for biofilm with an empirical formula $C_4H_7O_2NP$; CASINO simulation of the absorbed electron in the sample as a function of acceleration voltage; and EDS spectral assignments (PDF)

AUTHOR INFORMATION

Corresponding Author

Sung Joon Kim − *Department of Chemistry, Howard University, Washington, District of Columbia 20059, United States;* orcid.org/0000-0002-2007-6606; Email: sung.kim@howard.edu

https://doi.org/10.1021/acsomega.4c01168
ACS Omega 2024, 9, 37610−37620

Authors

Binayak Rimal − *Institute of Biomedical Studies, Baylor University, Waco, Texas 76798, United States*

James D. Chang − *Department of Chemistry and Biochemistry, Baylor University, Waco, Texas 76798, United States*

Chengyin Liu − *Department of Chemistry, Howard University, Washington, District of Columbia 20059, United States*

Haley Kim − *Department of Chemistry, University of Maryland, College Park, Maryland 20742, United States*

Oluwatobi Aderotoye − *Department of Chemistry, Howard University, Washington, District of Columbia 20059, United States*

Bernd Zechmann − *Center for Microscopy and Imaging, Baylor University, Waco, Texas 76798, United States*

Complete contact information is available at: https://pubs.acs.org/10.1021/acsomega.4c01168

Author Contributions

S.J.K., B.R., and J.C. prepared *S. aureus* biofilms. J.C., B.Z., and S.J.K. carried out SEM and EDS measurements. H.K. and C.L. performed CASINO simulations. All authors contributed to the writing of the manuscript.

Notes

The authors declare no competing financial interest.

■ ACKNOWLEDGMENTS

The authors would like to express thanks to Professor Friedrick Götz (University of Tübingen) for providing the *S. aureus* strain SA113 and Chloe Post and Jonah Kim for their assistance with the CASINO simulations. This work was supported by the National Institutes of Health grant number GM143682.

■ ABBREVIATIONS

EDS, energy-dispersive X-ray spectroscopy; LC−MS, liquid chromatography−mass spectrometry; WTA, wall teichoic acids; CASINO, Monte Carlo simulation of electron trajectories in solids; eDNA, extracellular DNA; PG, peptidoglycan; CPMAS, cross-polarization at magic angle spinning

■ REFERENCES

(1) Otto, M. Staphylococcal infections: mechanisms of biofilm maturation and detachment as critical determinants of pathogenicity. *Annu. Rev. Med.* **2013**, *64*, 175−188.

(2) Romanò, C. L.; Toscano, M.; Romano, D.; Drago, L. Antibiofilm agents and implant-related infections in orthopaedics: where are we? *J. Chemother.* **2013**, *25* (2), 67−80.

(3) Stewart, P. S.; Costerton, J. W. Antibiotic resistance of bacteria in biofilms. *Lancet* **2001**, *358* (9276), 135−138.

(4) Mayer, C.; Moritz, R.; Kirschner, C.; Borchard, W.; Maibaum, R.; Wingender, J.; Flemming, H. C. The role of intermolecular interactions: studies on model systems for bacterial biofilms. *Int. J. Biol. Macromol.* **1999**, *26* (1), 3−16.

(5) Foster, T. J. The MSCRAMM Family of Cell-Wall-Anchored Surface Proteins of Gram-Positive Cocci. *Trends Microbiol.* **2019**, *27* (11), 927−941.

(6) Patti, J. M.; Allen, B. L.; McGavin, M. J.; Hook, M. MSCRAMM-mediated adherence of microorganisms to host tissues. *Annu. Rev. Microbiol.* **1994**, *48*, 585−617.

(7) Geoghegan, J. A.; Corrigan, R. M.; Gruszka, D. T.; Speziale, P.; O'Gara, J. P.; Potts, J. R.; Foster, T. J. Role of surface protein SasG in biofilm formation by *Staphylococcus aureus*. *J. Bacteriol.* **2010**, *192* (21), 5663−5673.

(8) Christner, M.; Franke, G. C.; Schommer, N. N.; Wendt, U.; Wegert, K.; Pehle, P.; Kroll, G.; Schulze, C.; Buck, F.; Mack, D.; et al. The giant extracellular matrix-binding protein of Staphylococcus epidermidis mediates biofilm accumulation and attachment to fibronectin. *Mol. Microbiol.* **2010**, *75* (1), 187−207.

(9) Linnes, J. C.; Ma, H.; Bryers, J. D. Giant extracellular matrix binding protein expression in Staphylococcus epidermidis is regulated by biofilm formation and osmotic pressure. *Curr. Microbiol.* **2013**, *66* (6), 627−633.

(10) Büttner, H.; Perbandt, M.; Kohler, T.; Kikhney, A.; Wolters, M.; Christner, M.; Heise, M.; Wilde, J.; Weisselberg, S.; Both, A.; et al. A Giant Extracellular Matrix Binding Protein of Staphylococcus epidermidis Binds Surface-Immobilized Fibronectin via a Novel Mechanism. *mBio* **2020**, *11* (5), No. e01612-20.

(11) Merino, N.; Toledo-Arana, A.; Vergara-Irigaray, M.; Valle, J.; Solano, C.; Calvo, E.; Lopez, J. A.; Foster, T. J.; Penades, J. R.; Lasa, I. Protein A-mediated multicellular behavior in *Staphylococcus aureus*. *J. Bacteriol.* **2009**, *191* (3), 832−843.

(12) O'Neill, E.; Pozzi, C.; Houston, P.; Humphreys, H.; Robinson, D. A.; Loughman, A.; Foster, T. J.; O'Gara, J. P. A novel *Staphylococcus aureus* biofilm phenotype mediated by the fibronectin-binding proteins, FnBPA and FnBPB. *J. Bacteriol.* **2008**, *190* (11), 3835−3850.

(13) Lasa, I.; Penades, J. R. Bap: a family of surface proteins involved in biofilm formation. *Res. Microbiol.* **2006**, *157* (2), 99−107.

(14) Roche, F. M.; Massey, R.; Peacock, S. J.; Day, N. P.; Visai, L.; Speziale, P.; Lam, A.; Pallen, M.; Foster, T. J. Characterization of novel LPXTG-containing proteins of *Staphylococcus aureus* identified from genome sequences. *Microbiology* **2003**, *149* (3), 643−654.

(15) Ton-That, H.; Labischinski, H.; Berger-Bachi, B.; Schneewind, O. Anchor structure of staphylococcal surface proteins. III. Role of the FemA, FemB, and FemX factors in anchoring surface proteins to the bacterial cell wall. *J. Biol. Chem.* **1998**, *273* (44), 29143−29149.

(16) Foster, T. J.; Geoghegan, J. A.; Ganesh, V. K.; Höök, M. Adhesion, invasion and evasion: the many functions of the surface proteins of *Staphylococcus aureus*. *Nat. Rev. Microbiol.* **2014**, *12* (1), 49−62.

(17) Kim, S. J.; Chang, J.; Rimal, B.; Yang, H.; Schaefer, J. Surface proteins and the formation of biofilms by *Staphylococcus aureus*. *Biochim. Biophys. Acta, Biomembr.* **2018**, *1860* (3), 749−756.

(18) Flemming, H. C.; Neu, T. R.; Wozniak, D. J. The EPS matrix: the "house of biofilm cells". *J. Bacteriol.* **2007**, *189* (22), 7945−7947.

(19) Sugimoto, S.; Sato, F.; Miyakawa, R.; Chiba, A.; Onodera, S.; Hori, S.; Mizunoe, Y. Broad impact of extracellular DNA on biofilm formation by clinically isolated Methicillin-resistant and sensitive strains of *Staphylococcus aureus*. *Sci. Rep.* **2018**, *8* (1), No. 2254.

(20) Flemming, H. C.; Wingender, J. The biofilm matrix. *Nat. Rev. Microbiol.* **2010**, *8* (9), 623−633.

(21) Götz, F. Staphylococcus and biofilms. *Mol. Microbiol.* **2002**, *43* (6), 1367−1378.

(22) Brown, S.; Santa Maria, J. P., Jr.; Walker, S. Wall teichoic acids of gram-positive bacteria. *Annu. Rev. Microbiol.* **2013**, *67*, 313−336.

(23) Holland, L. M.; Conlon, B.; O'Gara, J. P. Mutation of tagO reveals an essential role for wall teichoic acids in Staphylococcus epidermidis biofilm development. *Microbiology* **2011**, *157* (2), 408−418.

(24) Gross, M.; Cramton, S. E.; Gotz, F.; Peschel, A. Key role of teichoic acid net charge in *Staphylococcus aureus* colonization of artificial surfaces. *Infect. Immun.* **2001**, *69* (5), 3423−3426.

(25) Wecke, J.; Madela, K.; Fischer, W. The absence of D-alanine from lipoteichoic acid and wall teichoic acid alters surface charge, enhances autolysis and increases susceptibility to methicillin in Bacillus subtilis. *Microbiology* **1997**, *143*, 2953−2960.

(26) Neuhaus, F. C.; Baddiley, J. A continuum of anionic charge: structures and functions of D-alanyl-teichoic acids in gram-positive bacteria. *Microbiol. Mol. Biol. Rev.* **2003**, *67* (4), 686−723.

(27) Ma, L.; Conover, M.; Lu, H.; Parsek, M. R.; Bayles, K.; Wozniak, D. J. Assembly and development of the Pseudomonas aeruginosa biofilm matrix. *PLoS Pathog.* **2009**, *5* (3), No. e1000354.
(28) Izano, E. A.; Amarante, M. A.; Kher, W. B.; Kaplan, J. B. Differential roles of poly-N-acetylglucosamine surface polysaccharide and extracellular DNA in *Staphylococcus aureus* and Staphylococcus epidermidis biofilms. *Appl. Environ. Microbiol.* **2008**, *74* (2), 470−476.
(29) Wingender, J.; Strathmann, M.; Rode, A.; Leis, A.; Flemming, H. C. Isolation and biochemical characterization of extracellular polymeric substances from Pseudomonas aeruginosa. *Methods Enzymol.* **2001**, *336*, 302−314.
(30) Wagner, M.; Ivleva, N. P.; Haisch, C.; Niessner, R.; Horn, H. Combined use of confocal laser scanning microscopy (CLSM) and Raman microscopy (RM): investigations on EPS-Matrix. *Water Res.* **2009**, *43* (1), 63−76.
(31) Allesen-Holm, M.; Barken, K. B.; Yang, L.; Klausen, M.; Webb, J. S.; Kjelleberg, S.; Molin, S.; Givskov, M.; Tolker-Nielsen, T. A characterization of DNA release in Pseudomonas aeruginosa cultures and biofilms. *Mol. Microbiol.* **2006**, *59* (4), 1114−1128.
(32) Periasamy, S.; Joo, H. S.; Duong, A. C.; Bach, T. H.; Tan, V. Y.; Chatterjee, S. S.; Cheung, G. Y.; Otto, M. How *Staphylococcus aureus* biofilms develop their characteristic structure. *Proc. Natl. Acad. Sci. U.S.A.* **2012**, *109* (4), 1281−1286.
(33) Friedman, L.; Kolter, R. Two genetic loci produce distinct carbohydrate-rich structural components of the *Pseudomonas aeruginosa* biofilm matrix. *J. Bacteriol.* **2004**, *186* (14), 4457−4465.
(34) Thurlow, L. R.; Hanke, M. L.; Fritz, T.; Angle, A.; Aldrich, A.; Williams, S. H.; Engebretsen, I. L.; Bayles, K. W.; Horswill, A. R.; Kielian, T. *Staphylococcus aureus* biofilms prevent macrophage phagocytosis and attenuate inflammation *in vivo*. *J. Immunol.* **2011**, *186* (11), 6585−6596.
(35) Boles, B. R.; Horswill, A. R. Agr-mediated dispersal of *Staphylococcus aureus* biofilms. *PLoS Pathog.* **2008**, *4* (4), No. e1000052.
(36) Demers, H.; Poirier-Demers, N.; Couture, A. R.; Joly, D.; Guilmain, M.; de Jonge, N.; Drouin, D. Three-dimensional electron microscopy simulation with the CASINO Monte Carlo software. *Scanning* **2011**, *33* (3), 135−146.
(37) Seidl, K.; Goerke, C.; Wolz, C.; Mack, D.; Berger-Bachi, B.; Bischoff, M. *Staphylococcus aureus* CcpA affects biofilm formation. *Infect. Immun.* **2008**, *76* (5), 2044−2050.
(38) Beenken, K. E.; Blevins, J. S.; Smeltzer, M. S. Mutation of sarA in *Staphylococcus aureus* limits biofilm formation. *Infect. Immun.* **2003**, *71* (7), 4206−4211.
(39) Khan, M. S. I.; Oh, S. W.; Kim, Y. J. Power of Scanning Electron Microscopy and Energy Dispersive X-Ray Analysis in Rapid Microbial Detection and Identification at the Single Cell Level. *Sci. Rep.* **2020**, *10* (1), No. 2368.
(40) Lee, S.; Choi, K. H.; Yoon, Y. Effect of NaCl on Biofilm Formation of the Isolate from *Staphylococcus aureus* Outbreak Linked to Ham. *Korean J. Food Sci. Anim. Resour.* **2014**, *34* (2), 257−261.
(41) Lee, S.; Kim, S.; Lee, H.; Ha, J.; Lee, J.; Choi, Y.; Oh, H.; Yoon, Y.; Choi, K. H. icaA Gene of *Staphylococcus aureus* Responds to NaCl, Leading to Increased Biofilm Formation. *J. Food Prot.* **2018**, *81* (3), 412−416.
(42) Trognon, J.; Rima, M.; Lajoie, B.; Roques, C.; El Garah, F. NaCl-induced modulation of species distribution in a mixed *P. aeruginosa*/*S. aureus*/*B. cepacia* biofilm. *Biofilm* **2023**, *6*, No. 100153.
(43) Körstgens, V.; Flemming, H. C.; Wingender, J.; Borchard, W. Influence of calcium ions on the mechanical properties of a model biofilm of mucoid Pseudomonas aeruginosa. *Water Sci. Technol.* **2001**, *43* (6), 49−57.
(44) Xia, G.; Kohler, T.; Peschel, A. The wall teichoic acid and lipoteichoic acid polymers of *Staphylococcus aureus*. *Int. J. Med. Microbiol* **2010**, *300* (2−3), 148−154.
(45) Weidenmaier, C.; Kokai-Kun, J. F.; Kristian, S. A.; Chanturiya, T.; Kalbacher, H.; Gross, M.; Nicholson, G.; Neumeister, B.; Mond, J. J.; Peschel, A. Role of teichoic acids in *Staphylococcus aureus* nasal colonization, a major risk factor in nosocomial infections. *Nat. Med.* **2004**, *10* (3), 243−245.
(46) Weidenmaier, C.; Peschel, A.; Xiong, Y. Q.; Kristian, S. A.; Dietz, K.; Yeaman, M. R.; Bayer, A. S. Lack of wall teichoic acids in *Staphylococcus aureus* leads to reduced interactions with endothelial cells and to attenuated virulence in a rabbit model of endocarditis. *J. Infect. Dis.* **2005**, *191* (10), 1771−1777.
(47) Whitchurch, C. B.; Tolker-Nielsen, T.; Ragas, P. C.; Mattick, J. S. Extracellular DNA required for bacterial biofilm formation. *Science* **2002**, *295* (5559), 1487.
(48) Steinberger, R. E.; Holden, P. A. Extracellular DNA in single- and multiple-species unsaturated biofilms. *Appl. Environ. Microbiol.* **2005**, *71* (9), 5404−5410.
(49) Rice, K. C.; Mann, E. E.; Endres, J. L.; Weiss, E. C.; Cassat, J. E.; Smeltzer, M. S.; Bayles, K. W. The cidA murein hydrolase regulator contributes to DNA release and biofilm development in *Staphylococcus aureus*. *Proc. Natl. Acad. Sci. U.S.A.* **2007**, *104* (19), 8113−8118.
(50) Houston, P.; Rowe, S. E.; Pozzi, C.; Waters, E. M.; O'Gara, J. P. Essential role for the major autolysin in the fibronectin-binding protein-mediated *Staphylococcus aureus* biofilm phenotype. *Infect. Immun.* **2011**, *79* (3), 1153−1165.
(51) Dengler, V.; Foulston, L.; DeFrancesco, A. S.; Losick, R. An Electrostatic Net Model for the Role of Extracellular DNA in Biofilm Formation by *Staphylococcus aureus*. *J. Bacteriol.* **2015**, *197* (24), 3779−3787.
(52) Gutiérrez, D.; Ruas-Madiedo, P.; Martinez, B.; Rodriguez, A.; Garcia, P. Effective removal of staphylococcal biofilms by the endolysin LysH5. *PLoS One* **2014**, *9* (9), No. e107307.
(53) Drouin, D.; Couture, A. R.; Joly, D.; Tastet, X.; Aimez, V.; Gauvin, R. CASINO V2.42: a fast and easy-to-use modeling tool for scanning electron microscopy and microanalysis users. *Scanning* **2007**, *29* (3), 92−101.

https://doi.org/10.1021/acsomega.4c01168
ACS Omega 2024, 9, 37610−37620